

~~CONFIDENTIAL~~

228

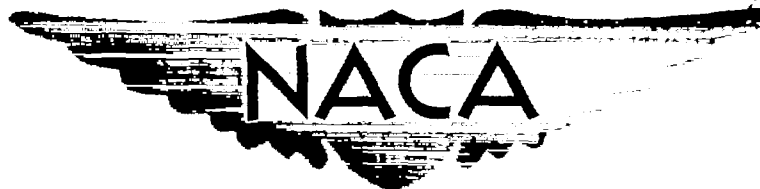
Copy  
RM L56G12

NACA RM L56G12

Re. # 13659

607 2 1956

0144254



# RESEARCH MEMORANDUM

ADDITIONAL RESULTS OF AN INVESTIGATION  
AT TRANSONIC SPEEDS TO DETERMINE THE EFFECTS OF A  
HEATED PROPULSIVE JET ON THE DRAG CHARACTERISTICS  
OF A SERIES OF RELATED AFTERBODIES

By Beverly Z. Henry, Jr., and Maurice S. Cahn

Langley Aeronautical Laboratory  
Langley Field, Va.

CLASSIFIED DOCUMENT

This material contains information affecting the National Defense of the United States within the meaning of the espionage laws, Title 18, U.S.C., Secs. 793 and 794, the transmission or revelation of which in any manner to an unauthorized person is prohibited by law.

## NATIONAL ADVISORY COMMITTEE FOR AERONAUTICS

WASHINGTON

September 24, 1956

~~CONFIDENTIAL~~

~~CONFIDENTIAL~~

0144254

## NATIONAL ADVISORY COMMITTEE FOR AERONAUTICS

## RESEARCH MEMORANDUM

ADDITIONAL RESULTS OF AN INVESTIGATION  
AT TRANSONIC SPEEDS TO DETERMINE THE EFFECTS OF A  
HEATED PROPULSIVE JET ON THE DRAG CHARACTERISTICS  
OF A SERIES OF RELATED AFTERBODIES

By Beverly Z. Henry, Jr., and Maurice S. Cahn

## SUMMARY

An investigation has been conducted at transonic speeds to determine the effects of a propulsive jet on the flow over the body from which it issues as influenced by changes in afterbody geometry. This paper is an extension, with limited analysis, of the work previously reported in NACA Research Memorandum L55A24a.

The results indicate that the effect on afterbody drag of increasing jet pressure ratio would be favorable on bodies with large extents of low angle boattailing and large jet-to-base diameter ratios and unfavorable on bodies of small extents of boattailing and small jet-to-base diameter ratios. This unfavorable effect existed on bodies with small jet-to-base diameter ratios even though the angle of boattailing was considered of favorable magnitude. Increasing jet temperature resulted in decreases in afterbody drag coefficient; this reduction was insignificant for the low-drag bodies but became significant for bodies of blunt shape. Increasing stream Mach number caused no change in jet effects for the low-drag bodies, whereas for the more blunt bodies there was a slight trend toward increased jet effects.

## INTRODUCTION

A previous investigation conducted in the Langley 8-foot transonic tunnel (ref. 1) to evaluate some of the effects of a sonic propulsive jet as influenced by changes in afterbody geometry indicated the desirability of studies extending this research to bodies with lower boattail angle and small jet-to-base diameter ratios. The results presented herein are therefore a continuation of the work reported in reference 1

~~CONFIDENTIAL~~

~~CONFIDENTIAL~~

and were obtained in an identical manner. The investigation was conducted at an angle of attack of  $0^\circ$  through the Mach number range from 0.80 to 1.10, and at each point the jet temperature and pressure ratio were varied.

Presented in this report are the basic data obtained from the investigation. The data are presented with limited analysis in order to expedite their availability to those concerned with jet-exit—afterbody design.

## SYMBOLS

A	area
$C_D$	drag coefficient, $\sum \frac{C_p A_l}{A_{\max}}$
$P_t$	total pressure
$l$	length
M	Mach number
$C_p$	pressure coefficient, $\frac{P_l - P_\infty}{q_\infty}$
R	Reynolds number, based on body length
$t$	total temperature, $^\circ F$
$d$	diameter
$p$	static pressure
$q$	dynamic pressure, $\frac{\gamma}{2} \rho M^2$
$\beta$	afterbody boattail angle, deg
$\gamma$	ratio of specific heats

## Subscripts:

A	afterbody
b	base

~~CONFIDENTIAL~~

j           jet  
 $\infty$           free stream  
 $\beta$           boattail  
l           local  
max         model maximum

## APPARATUS AND TESTS

### Wind Tunnel

This investigation was conducted in the Langley 8-foot transonic tunnel which has a dodecagonal slotted test section that permitted continuous testing up to a Mach number of approximately 1.10 for these models. The tunnel is vented to the atmosphere through an air exchange tower which permits the exhausting of combustion gases from the model into the stream with no detrimental effects on the characteristics of the stream. Details of the test section are presented in reference 2. Aerodynamic characteristics of the airstream are given in reference 3 wherein it is shown that the maximum deviation from the indicated free-stream Mach number is  $\pm 0.003$ .

### Models

The models used in the investigation were bodies of revolution, the rear portions of which were removed to provide an exit for the jet. These bodies had fineness ratios from 10.0 to 10.6. A single forebody (see table I) was used throughout the investigation and the model design allowed the ready interchange of afterbodies of various geometric shapes. The models were mounted in the tunnel by means of two support struts. These support struts, with a chord of 11.25 inches and an NACA 65-010 airfoil section measured parallel to the airstream, were placed so that the leading edge intersected the body at a point 21.7 inches from the nose and were swept back  $45^\circ$ . A sketch of the general arrangement of the model in the tunnel is shown in figure 1. For all tests the nose of the model was located 46 inches downstream of the slot origin.

Presented in table II is the equation utilized to define the external shapes of the afterbodies investigated. Also shown are the design points used to assign values to the equation. The ordinates from which the body shapes were constructed are given in table I. Drawings of the afterbody shapes are shown in figure 2. The models were instrumented

with base pressure orifices and with three rows of static-pressure orifices at  $0^\circ$ ,  $45^\circ$ , and  $72^\circ$  from the plane of symmetry.

### Turbojet Simulator

Contained within the models was a device for the simulation of a turbojet exhaust. To satisfy the simulation requirements a combustor was developed which burns a mixture of ethylene and air and exhausts the combustion products through a sonic nozzle. The combustion products of such a mixture possess physical and thermodynamic characteristics comparable to those of a nonafterburning turbojet exhaust. Jet pressure ratio was varied by changes in mass flow to the simulator and jet temperature was varied by changes in fuel-air ratio. Physical details of the simulator are presented in reference 1.

### Tests and Measurements

For this investigation, the models were tested at an angle of attack of  $0^\circ$  through the Mach number range from 0.80 to 1.10. At each test Mach number, the jet pressure ratio was varied from a no-flow condition to 11 or to the maximum obtainable at jet temperatures of "cold,"  $800^\circ\text{F}$ , and  $1,200^\circ\text{F}$ . The term "cold" flow is used herein to define the temperature of the air coming from the source, normally  $75^\circ$  to  $80^\circ\text{F}$ , and corresponds to a fuel-air ratio of 0. The Reynolds number based on body length varied from  $15.0 \times 10^6$  to  $17.4 \times 10^6$  (see fig. 3).

At each test point, body-pressure distributions, base pressures, and free-stream test conditions were photographically recorded from multiple-tube manometers. Tunnel total temperature was obtained from a recording potentiometer.

Rates of flow of fuel and air were determined by use of standard ASME sharp-edge-orifice flowmeters. Jet total pressure was obtained from a calibrated probe mounted in the combustion chamber and was referenced to a static-pressure orifice on the tunnel wall for the determination of jet pressure ratio. Jet temperature was obtained from a shielded chromel-alumel thermocouple near the exit station. All values defining the jet condition were photographically recorded by a camera synchronized with that used to record pressure data.

## RESULTS

The basic results of the investigation are presented in figures 4 and 5. Presented are base pressure coefficients and afterbody pressure-drag coefficients as a function of jet pressure ratio for various Mach numbers and at jet temperatures of cold, 800°, and 1,200° F. The drag-coefficient values have been presented in component and total forms to indicate the relative contribution of the body, boattail, and base to total afterbody pressure drag. Values of afterbody-pressure-drag coefficient were obtained by numerical integration of body pressures and are based on body frontal area. For the cylindrical afterbodies X and XIV (figs. 5(c) and 5(g)) only total-drag-coefficient values are presented since for these cases  $C_{D,b} = C_{D,A}$ . Base-pressure-drag coefficient was determined in all cases, including the no-flow condition, from the pressure acting on the base annulus area. Separate figures are presented for each afterbody.

Very low jet pressure ratios corresponding to base bleed conditions were investigated for afterbodies X and XI which represent the geometric extremes of the shapes studied. Afterbody X is cylindrical in shape with the resulting large base annulus, whereas afterbody XI has a small base annulus and a large extent of boattailing. These small amounts of jet flow resulted in drag reductions for each afterbody (fig. 5(c) and fig. 5(d)). In the presentation of results obtained from the other afterbody shapes investigated, no curves have been faired between the no-flow point and a jet pressure ratio of 2. It may reasonably be assumed, however, that the variation will be similar to that presented for afterbodies X and XI.

Additional tests were made of afterbodies I and VII to extend and clarify results originally obtained with these bodies and presented in reference 1. The results for afterbody I contained herein include measurements obtained at a jet temperature of 800° F which were not available previously. The later study of afterbody VII was conducted to clarify the questionable results obtained at a jet temperature of 800° F as noted in reference 1. Since the results herein presented showed no unusual variation of the jet effect with changes in jet temperature, it was concluded that errors were induced in the previous 800° F data by incorrect setting of the tunnel diffuser entrance ramps. This improper setting would cause no change in the nature of the jet effect but would result in a change in the afterbody drag level for this model due to small increases in local static pressure near the rear of the body (see ref. 4).

Afterbody XI,  $\beta = 8^\circ$ ,  $d_j/d_b = 0.742$ , extends the range of geometric variables available in reference 1 to indicate the influence of afterbody

boattail angle on the effects of the jet. Afterbodies XII and XIII,  $\beta = 16^\circ$ , and  $d_j/d_b = 0.388$  and  $0.336$ , respectively, extend the range of base sizes studied in reference 1 with the cylindrical afterbody X,  $d_j/d_b = 0.248$ , representing the end point in this variation.

For the tests made at a Mach number of 1.10 a disturbance originating at the support-body juncture was reflected from the tunnel wall to intersect the model at a point approximately 2.5 jet diameters upstream of the base. While the presence of this reflected disturbance resulted in more positive local pressures, and consequently in lower drag values, examination of the results indicated no change in the jet effects which could be attributed to such a disturbance.

### DISCUSSION

The results obtained in this investigation coincide with the trends evidenced by the work of reference 1. Small jet-flow quantities corresponding to a base-bleed condition result in an initial reduction in drag. Increasing jet pressure ratio above the base-bleed condition to about 3 results in a drag increase. As the jet pressure ratio is increased above this point, the influence of afterbody configuration becomes more important. For the low-drag shapes, bodies with extensive low-angle boattailing ( $8^\circ$  to  $16^\circ$ ) and small base annulus sizes ( $d_j/d_b \approx 0.5$  or larger), increasing jet pressure ratio results in drag reductions. For the blunt shapes, bodies with lesser extent of boattailing and large base sizes ( $d_j/d_b < 0.5$ ), unfavorable drag changes occurred with increases in jet pressure ratio even though the boattail angle was of a favorable magnitude ( $16^\circ$ ). The range of jet pressure ratio through which this unfavorable effect occurs increases with decreases in jet-to-base diameter ratio as may be seen by comparing afterbodies X, XI, and XII.

As the jet pressure ratio is increased above a value of about 2, the jet expands externally. When this expansion has increased to a point where interaction with the external stream occurs, an outward deflection of the external stream results with an accompanying compression in the region of the body base and a corresponding reduction in afterbody drag. On bodies with large extents of low-angle boattailing and small base annulus sizes, such as afterbodies I and XI, this effect is felt at a pressure ratio of about 3. Afterbodies X, XII, XIII, and XIV, however, have base annuli of sufficient size that the predominant effect of the jet within the range of this investigation is to aspirate these large low-energy regions, with a resulting increase in drag. At higher pressure ratios, the jet would be expected to expand sufficiently for the interaction with the external stream to cause a reversal in the drag variation. An example of this phenomena may be found in reference 5.

~~CONFIDENTIAL~~

The effect of increasing jet temperature at a constant value of jet pressure ratio was to reduce the afterbody drag. For the bodies with large extents of favorable boattailing and small base sizes the effects of changes in jet temperature were so small as to be considered negligible. For those bodies with large bases and small extents of boattailing the effects of changes in jet temperature became significant with the largest effect being noted on the cylindrical configurations.

Mach number changes in the range of this investigation resulted in no major variation in the character of the jet effects. The effect of the jet remained essentially constant with changes in Mach number for those bodies with large extents of favorable boattailing and small base sizes. For those bodies with small extents of boattailing and large base sizes, a trend toward increased jet effects as the Mach number was increased was noted.

#### SUMMARY OF RESULTS

From the results of an investigation at transonic speeds to determine the effect of a propulsive jet on the body from which it issues as influenced by changes in afterbody geometry, the following observations are made:

1. The effect on afterbody drag of increasing jet pressure ratio was favorable on bodies with large extents of low-angle boattailing and small base annulus sizes and unfavorable on bodies with small extents of boattailing and large base annulus sizes.
2. Decreasing jet-to-base diameter ratio below about 0.5 resulted in unfavorable jet effects through a range of jet pressure ratios which increased as jet-to-base diameter ratio decreased even though the angle of boattailing was of a favorable magnitude.
3. The effect of increasing jet temperature at a constant jet pressure ratio was to cause a reduction in drag coefficient. This reduction was insignificant for the low-drag bodies but became significant for bodies of blunt shape.

~~CONFIDENTIAL~~



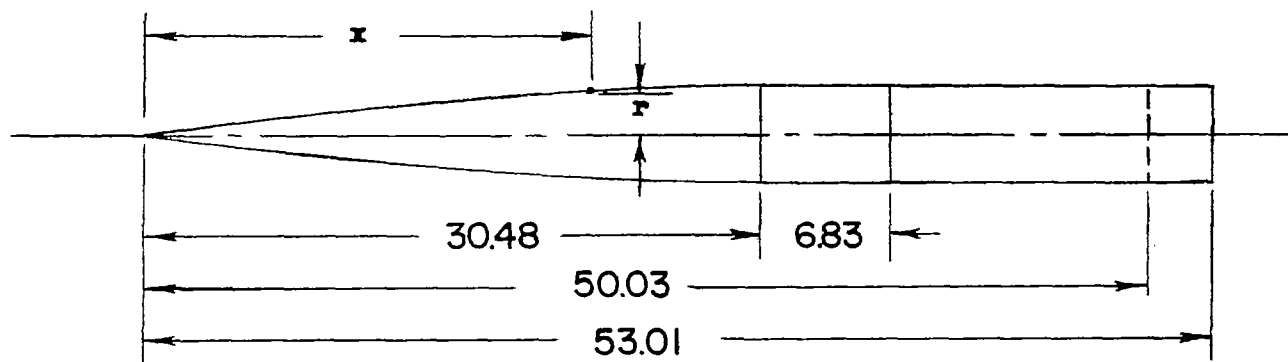
4. In the range of this investigation, increasing stream Mach number caused no change in the jet effects on the low-drag shapes, whereas for the blunt bodies there was a trend toward increased jet effects.

Langley Aeronautical Laboratory,  
National Advisory Committee for Aeronautics,  
Langley Field, Va., June 22, 1956.

#### REFERENCES

1. Henry, Beverly Z., Jr., and Cahn, Maurice S.: Preliminary Results of an Investigation at Transonic Speeds To Determine the Effects of a Heated Propulsive Jet on the Drag Characteristics of a Related Series of Afterbodies. NACA RM L55A24a, 1955.
2. Wright, Ray H., and Ritchie, Virgil S.: Characteristics of a Transonic Test Section With Various Slot Shapes in the Langley 8-Foot High-Speed Tunnel. NACA RM L51H10, 1951.
3. Ritchie, Virgil S., and Pearson, Albin O.: Calibration of the Slotted Test Section of the Langley 8-Foot Transonic Tunnel and Preliminary Experimental Investigation of Boundary-Reflected Disturbances. NACA RM L51K14, 1952.
4. Whitcomb, Richard T., Carmel, Melvin M., and Morgan, Francis G., Jr.: An Investigation of the Stream-Tube Power Losses and an Improvement of the Diffuser-Entrance Nose in the Langley 8-Foot Transonic Tunnel. NACA RM L52E20, 1952.
5. Cabbage, James M., Jr.: Jet Effects on Base and Afterbody Pressures of a Cylindrical Afterbody at Transonic Speeds. NACA RM L56C21, 1956.

TABLE I  
BODY ORDINATES



Forebody Ordinates

Station, x, in.	Radius	Station, x, in.	Radius
0.30	0.139	12.00	1.854
.45	.179	15.00	2.079
.75	.257	18.00	2.245
1.50	.433	21.00	2.360
3.00	.723	24.00	2.438
4.50	.968	27.00	2.486
6.00	1.183	30.00	2.500
9.00	1.556	30.48	2.500

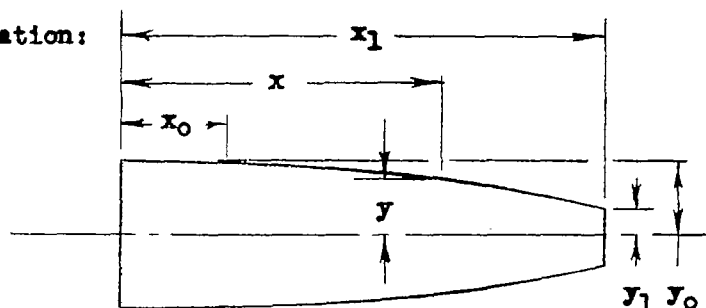
Afterbody Ordinates

Station, x, in.	Radius, r, in.						
	I	VII	X	XI	XII	XIII	XIV
30.48	2.500	2.500	2.500	2.500	2.500	2.500	2.500
37.31	2.500	2.500	---	2.500	---	---	---
40.12	2.500	2.500	---	2.500	---	---	---
42.12	2.469	2.492	---	2.278	---	---	---
44.12	2.364	2.419	---	2.030	---	---	---
46.12	2.176	2.260	---	1.772	2.500	2.500	---
48.12	1.901	2.006	---	1.506	2.432	2.499	---
50.03	---	---	---	---	---	---	2.500
50.12	1.534	1.654	---	1.235	2.214	2.392	---
51.12	1.315	1.440	---	1.098	2.043	2.259	---
52.12	1.073	1.201	---	.960	1.828	2.067	---
53.01	.836	.965	2.500	.836	1.600	1.845	---

Table II

## AFTERBODY DESIGN

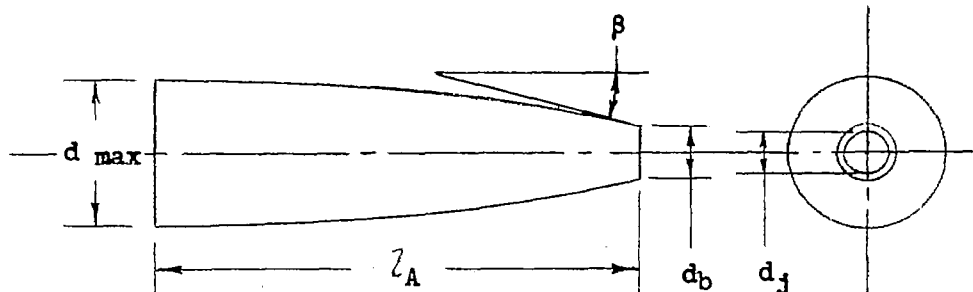
Equation:



$$y = y_0 - (y_0 - y_1) \left( \frac{x - x_0}{x_1 - x_0} \right)^{\left( \frac{x_1 - x_0}{y_0 - y_1} \right) \tan \beta}$$

where:  $x$  = any afterbody station  
 $x_1$  = body base station  
 $x_0$  = body tangency point  
 $y$  = radius at station  $x$   
 $y_1$  = body base radius  
 $y_0$  = maximum body radius  
 $\beta$  = boattail angle  
 $\frac{x_1 - x_0}{y_0 - y_1} = \text{constant} = 7.747$

Design points:



Afterbody	$d_{\max}$ , in.	$l_A$ , in.	$\beta$ , deg	$d_j$ , in.	$d_b$ , in.	$d_j/d_b$	$d_j/d_{\max}$
I	5.0	15.70	16	1.240	1.672	0.742	0.248
VII	5.0	15.70	16	1.240	1.930	0.643	0.248
X	5.0	15.70	0	1.240	5.00	0.248	0.248
XI	5.0	15.70	8	1.240	1.672	0.742	0.248
XII	5.0	15.70	16	1.240	3.200	0.388	0.248
XIII	5.0	15.70	16	1.240	3.690	0.336	0.248
XIV	5.0	12.72	0	1.754	5.00	0.351	0.351

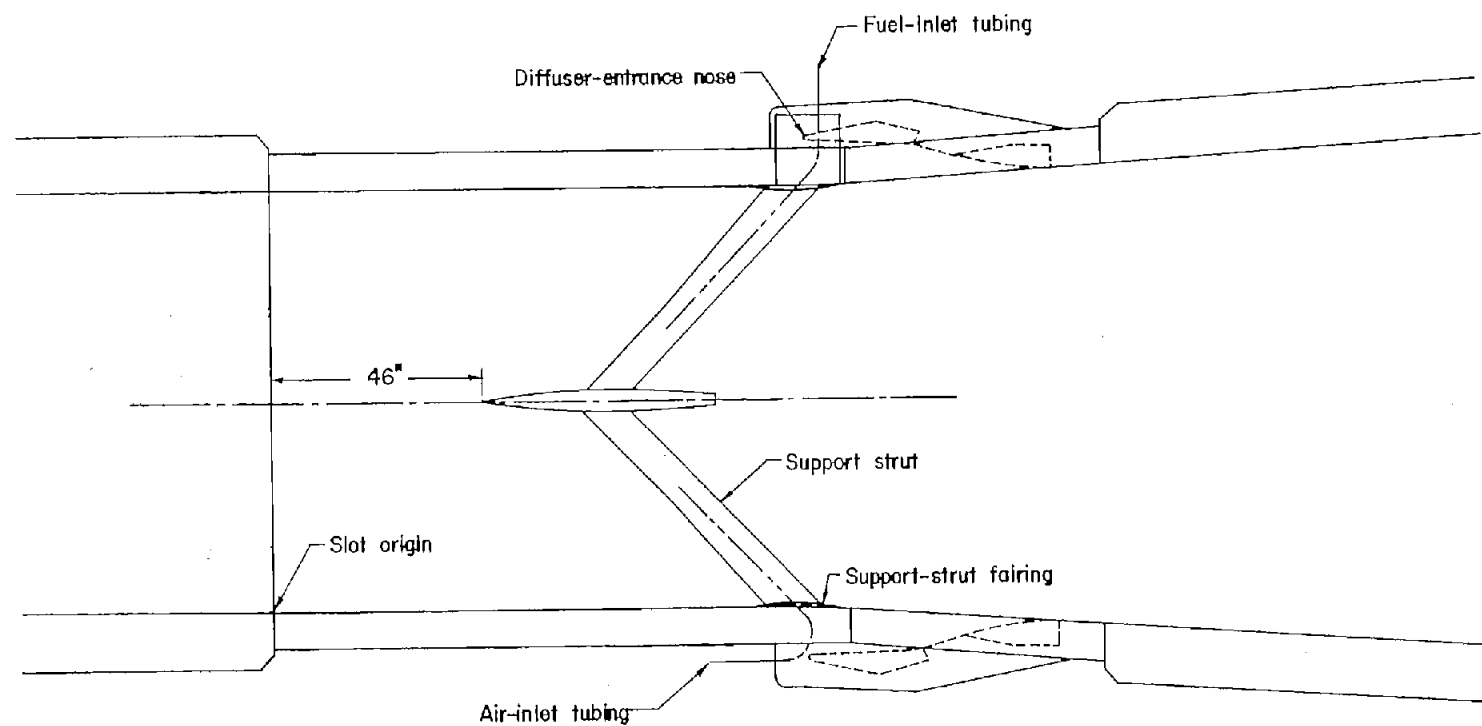


Figure 1.- Turbojet-simulator model in Langley 8-foot transonic tunnel.

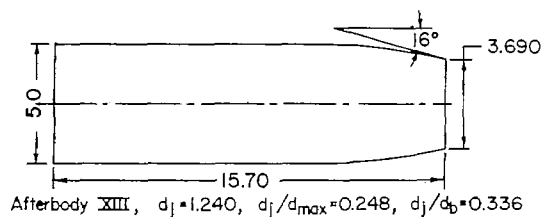
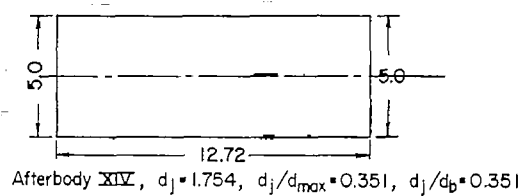
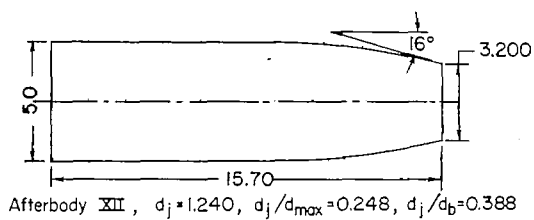
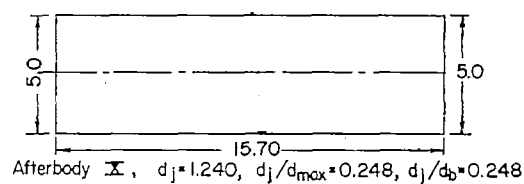
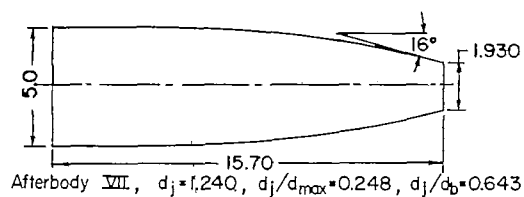
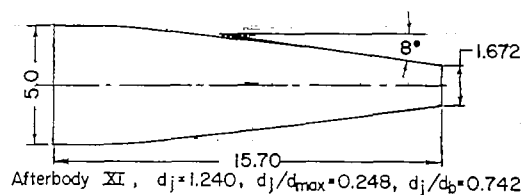
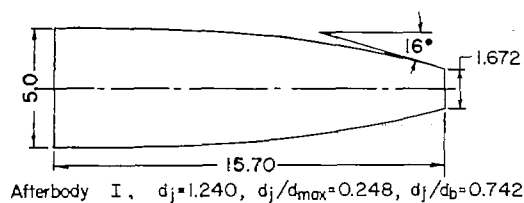


Figure 2.- Afterbody shapes investigated. All dimensions are in inches unless otherwise stated.

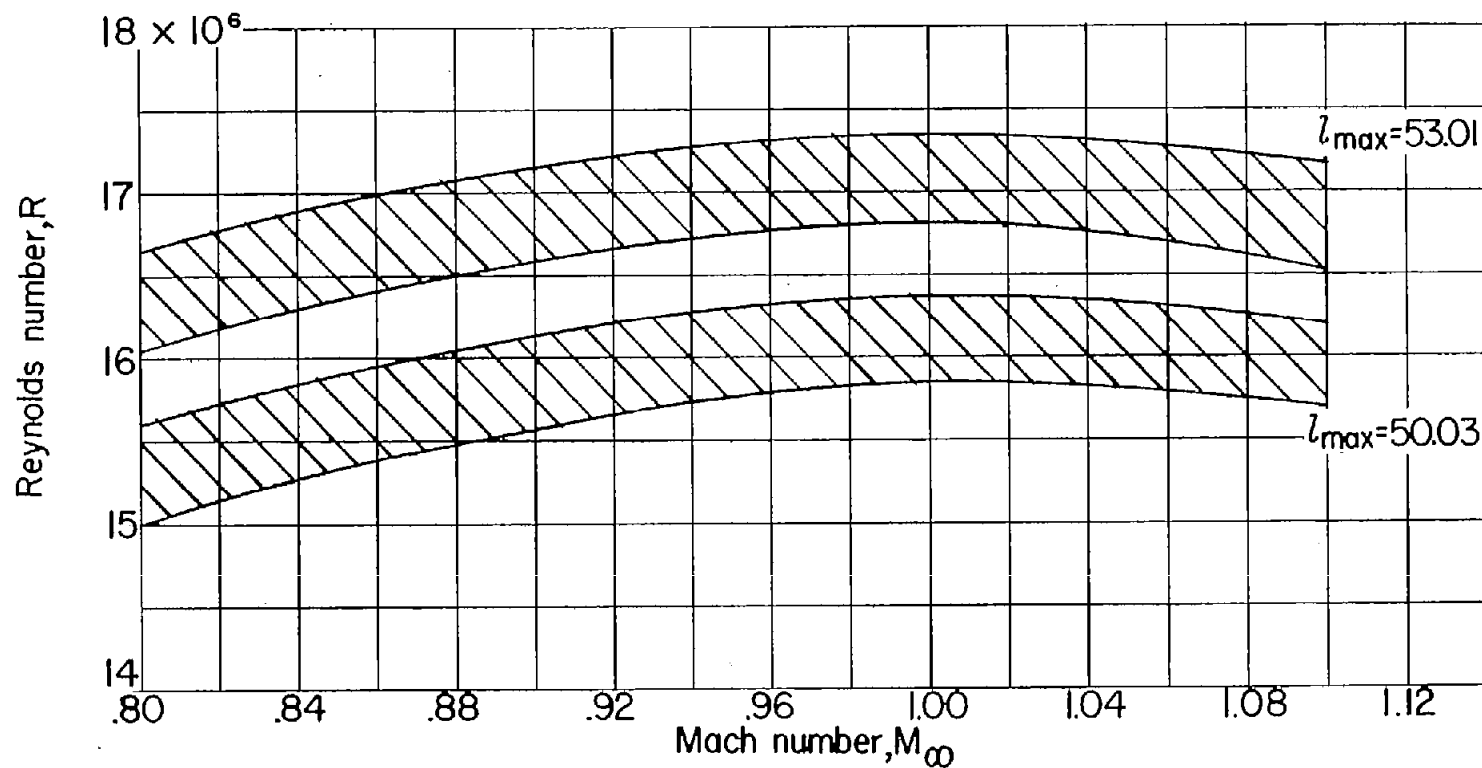
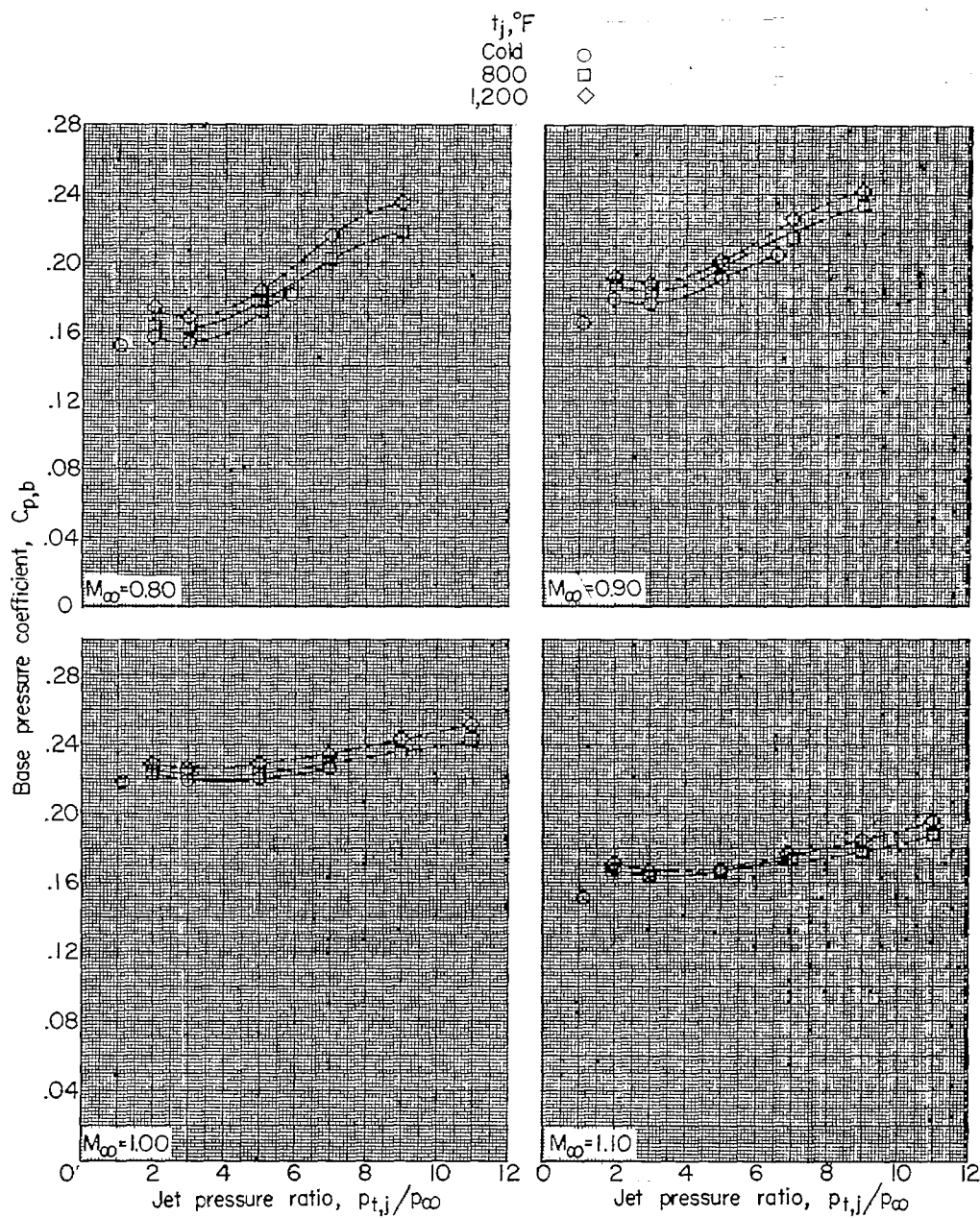


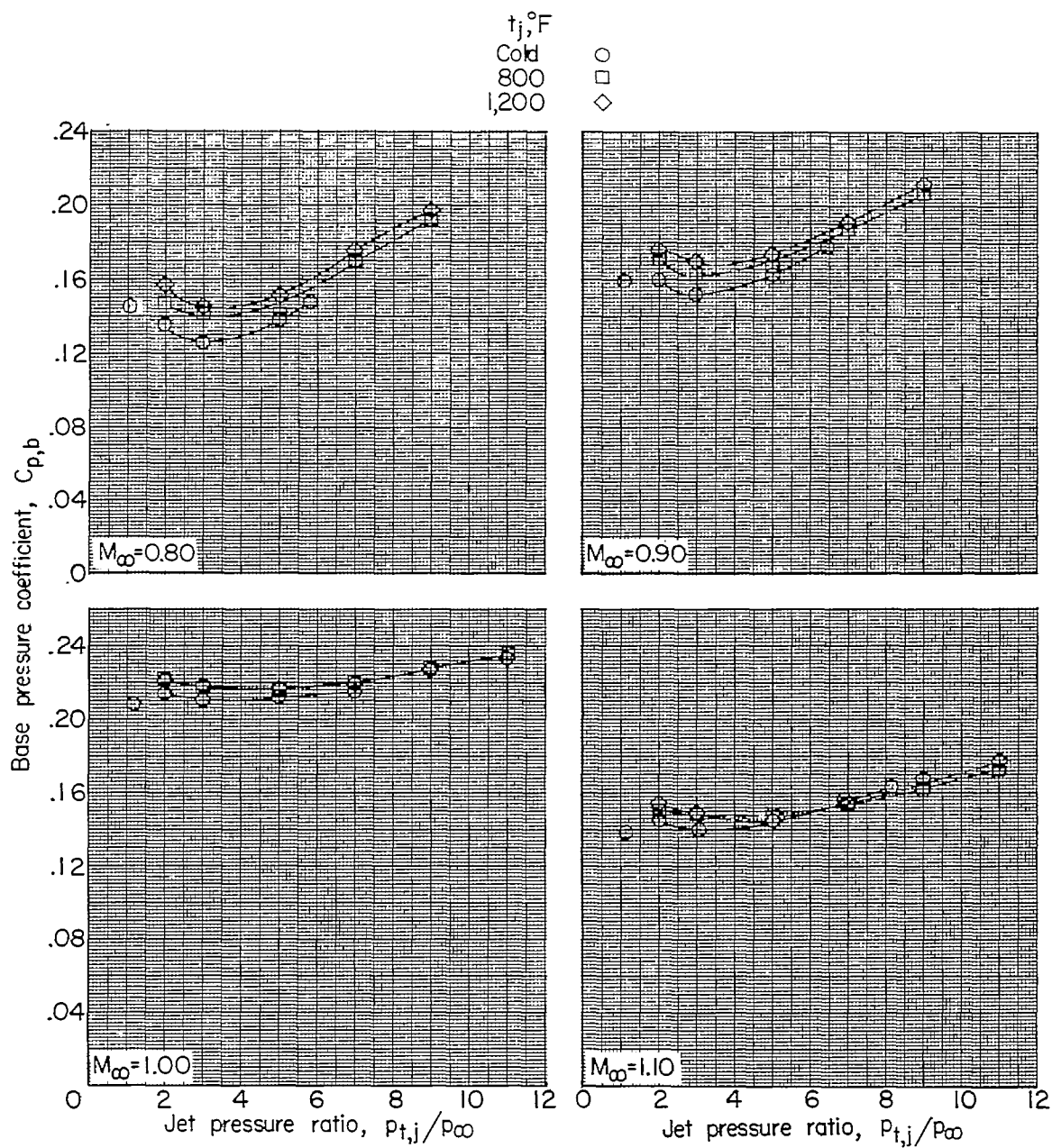
Figure 3.- Variation of Reynolds number, based on body length, with Mach number.

~~CONFIDENTIAL~~

(a) Afterbody I.  $\beta = 16^\circ$ ,  $\frac{d_j}{d_{\max}} = 0.248$ ,  $\frac{d_j}{d_b} = 0.742$ .

Figure 4.- Variation of base pressure coefficient with jet pressure ratio at different values of jet temperature and stream Mach number.

~~CONFIDENTIAL~~

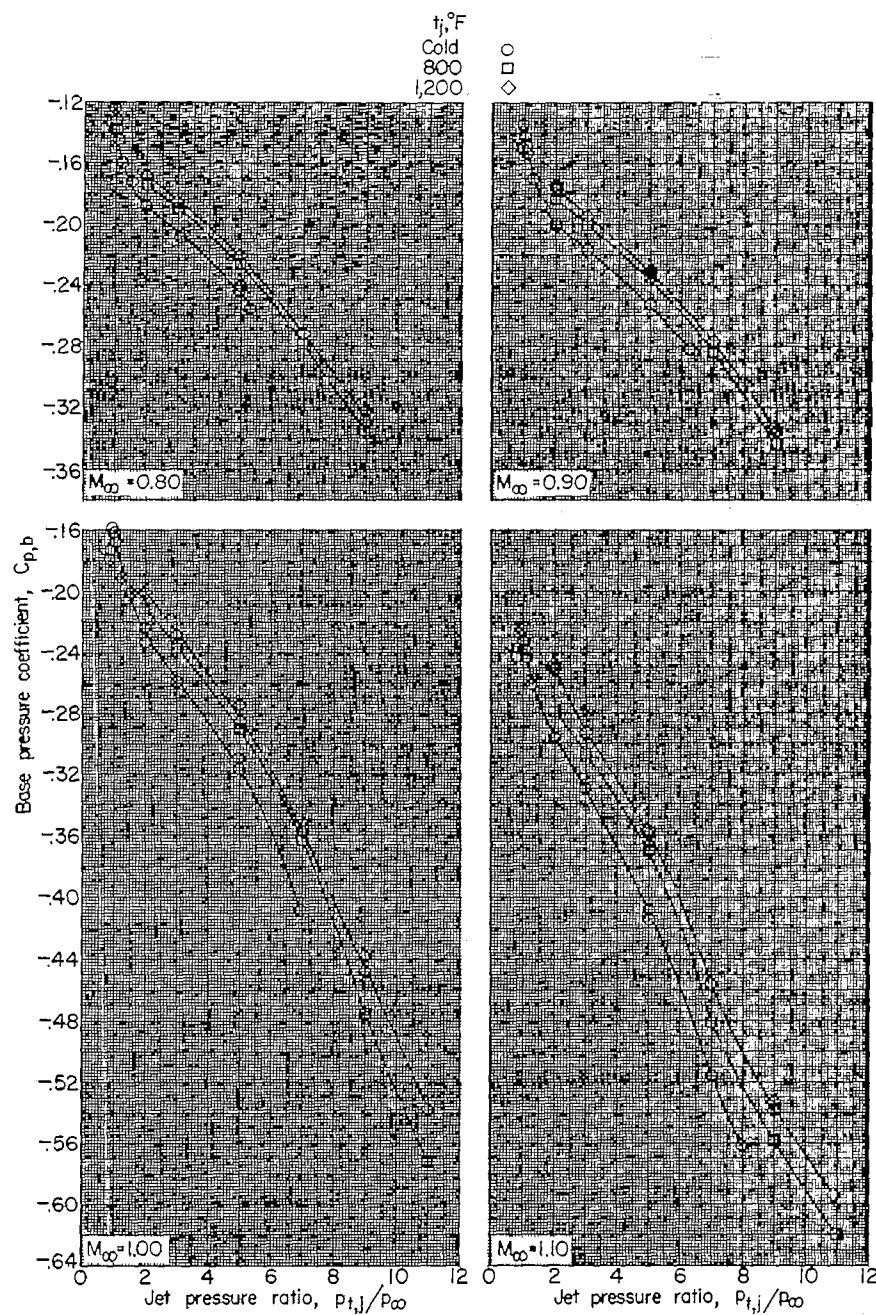


(b) Afterbody VII.  $\beta = 16^\circ$ ,  $\frac{d_j}{d_{\max}} = 0.248$ ,  $\frac{d_j}{d_b} = 0.643$ .

Figure 4.- Continued.

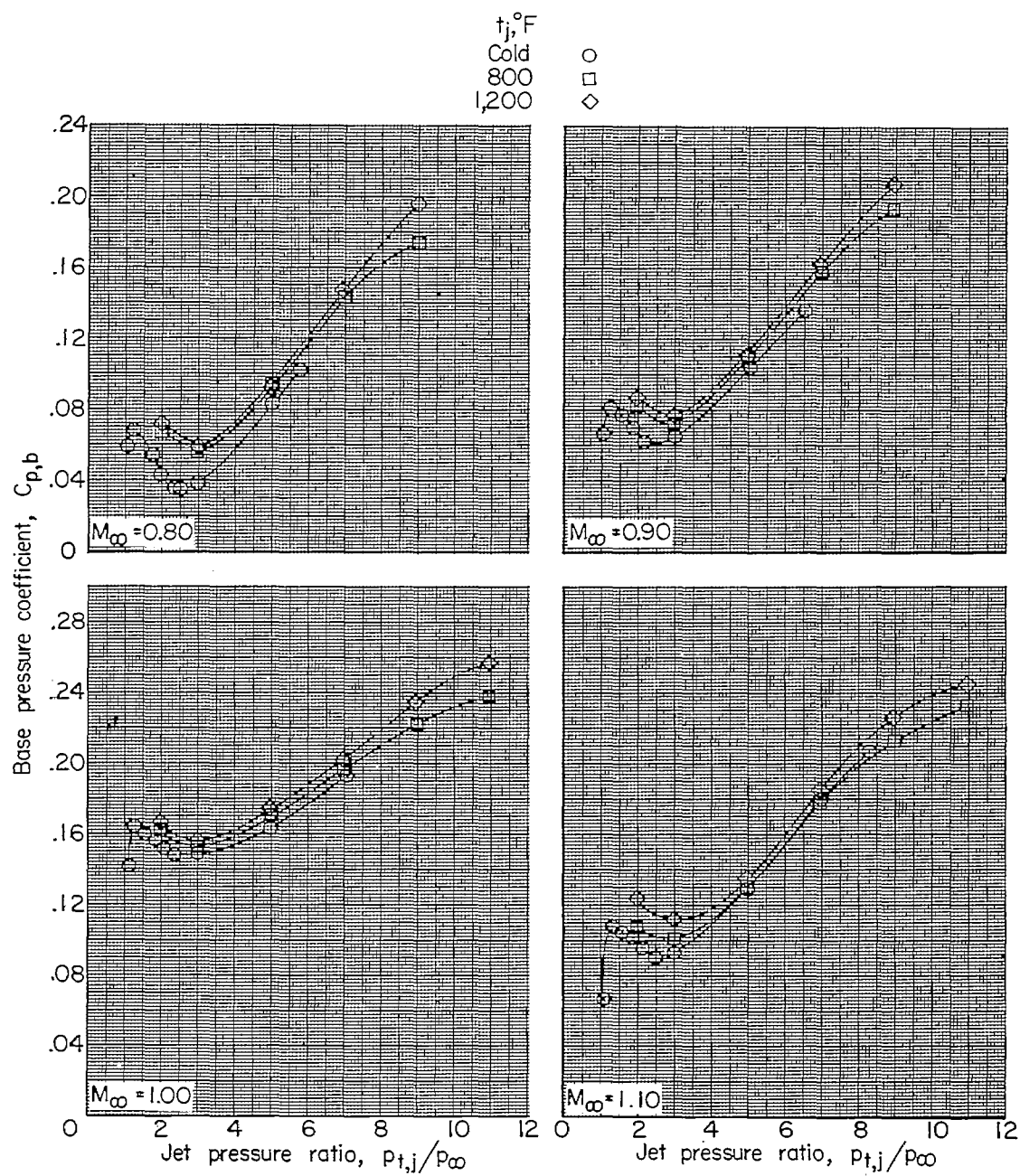
CONFIDENTIAL





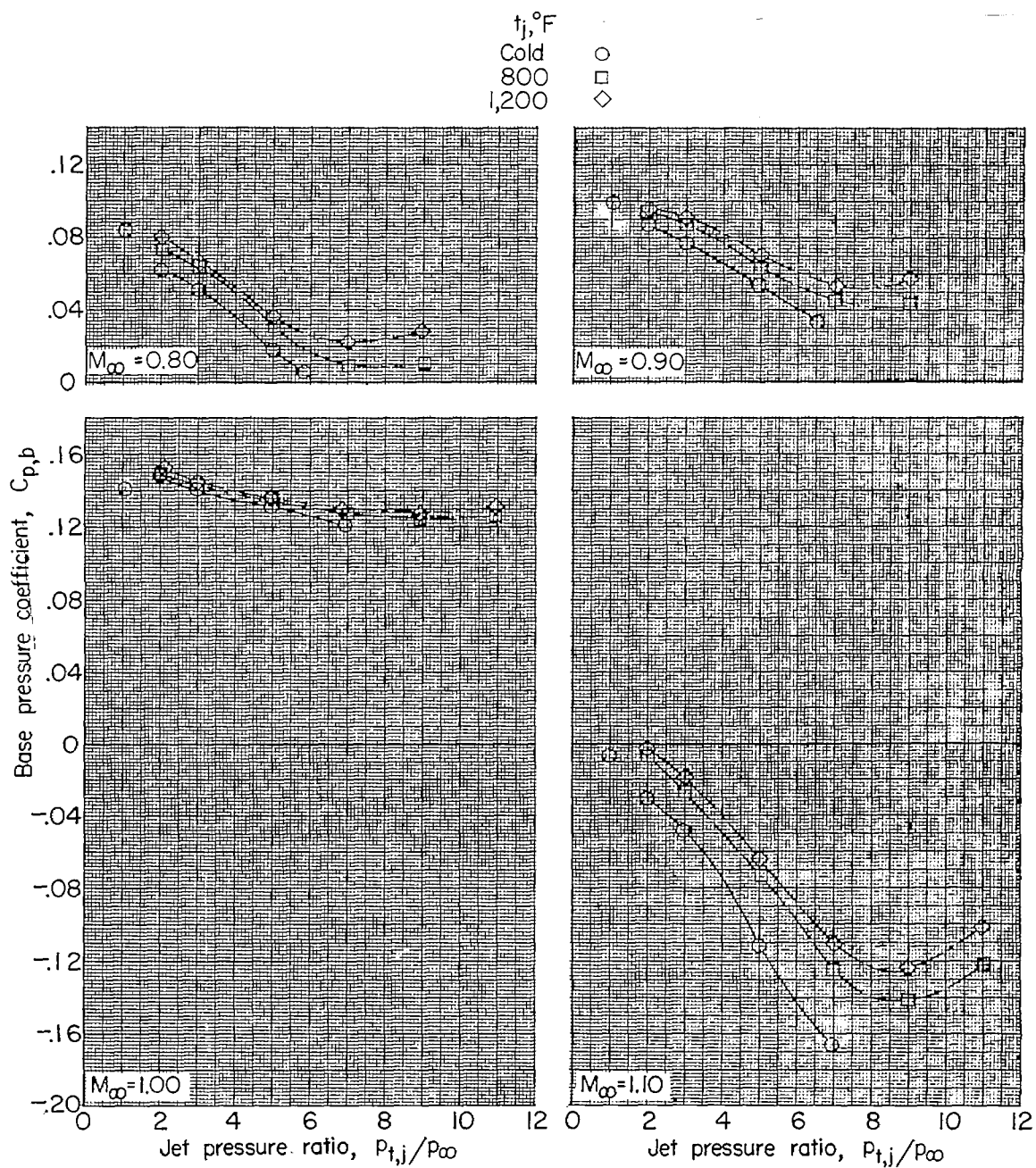
(c) Afterbody X.  $\beta = 0^\circ$ ,  $\frac{d_j}{d_{\max}} = 0.248$ ,  $\frac{d_j}{d_b} = 0.248$ . Flagged symbols are for no jet flow.

Figure 4.- Continued.



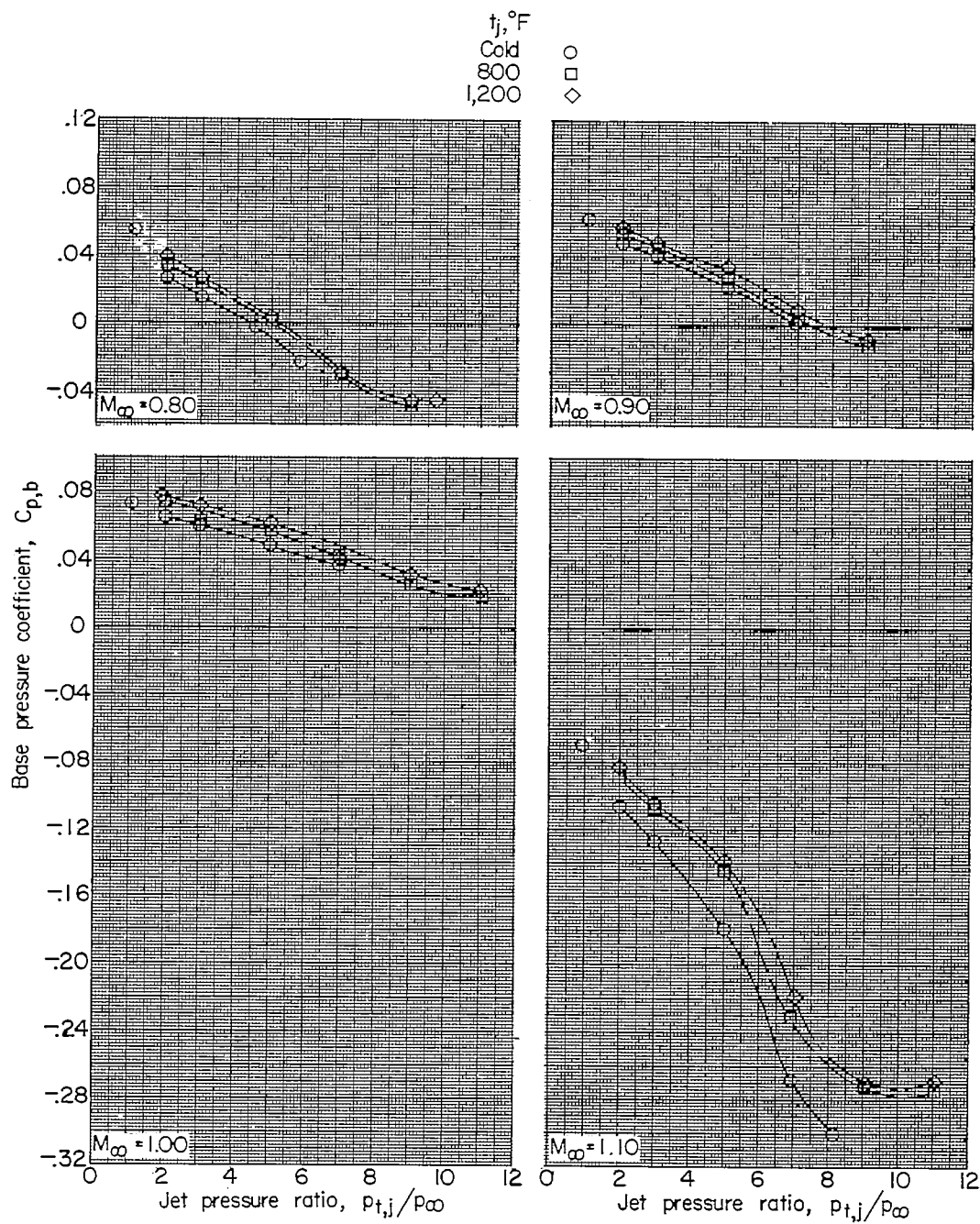
(d) Afterbody XI.  $\beta = 8^\circ$ ,  $\frac{d_j}{d_{max}} = 0.248$ ,  $\frac{d_j}{d_b} = 0.742$ .

Figure 4.- Continued.



(e) Afterbody XIII.  $\beta = 16^\circ$ ,  $\frac{d_j}{d_{\max}} = 0.248$ ,  $\frac{d_j}{d_b} = 0.388$ .

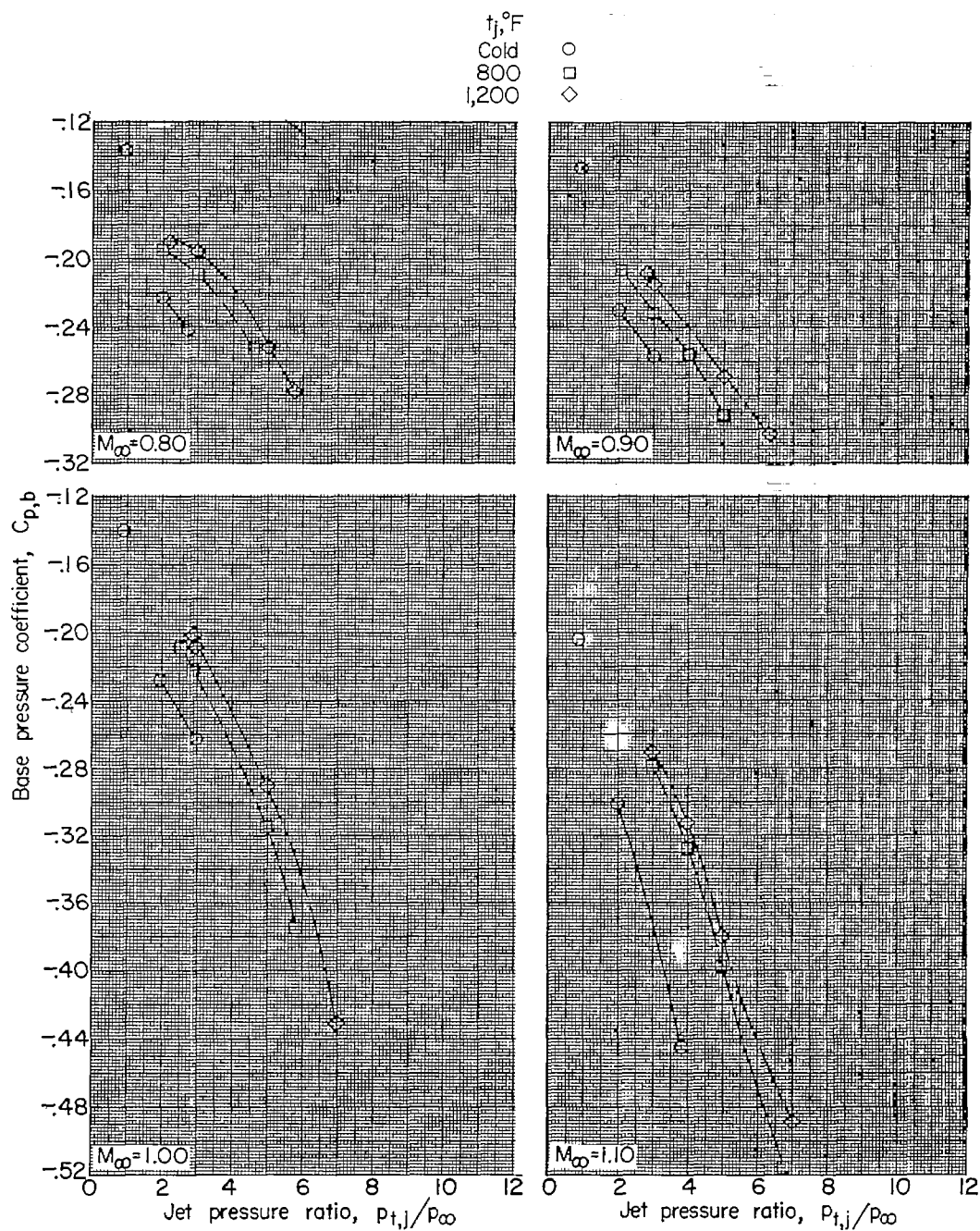
Figure 4.- Continued.

~~CONFIDENTIAL~~

(f) Afterbody XIII.  $\beta = 16^\circ$ ,  $\frac{d_j}{d_{max}} = 0.248$ ,  $\frac{d_j}{d_b} = 0.336$ .

Figure 4.- Continued.

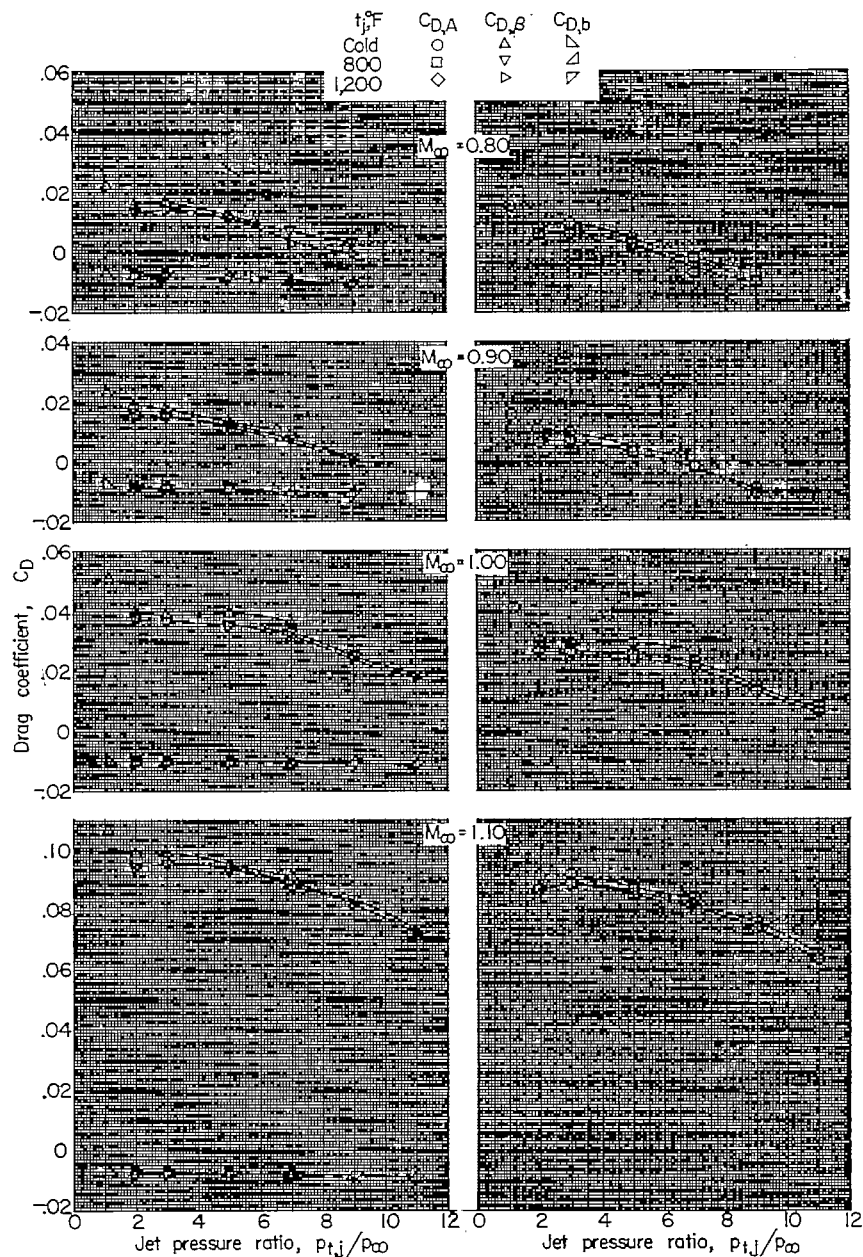
~~CONFIDENTIAL~~

~~CONFIDENTIAL~~

(g) Afterbody XIV.  $\beta = 0^\circ$ ,  $\frac{d_j}{d_{\max}} = 0.351$ ,  $\frac{d_j}{d_b} = 0.351$ .

Figure 4.- Concluded.

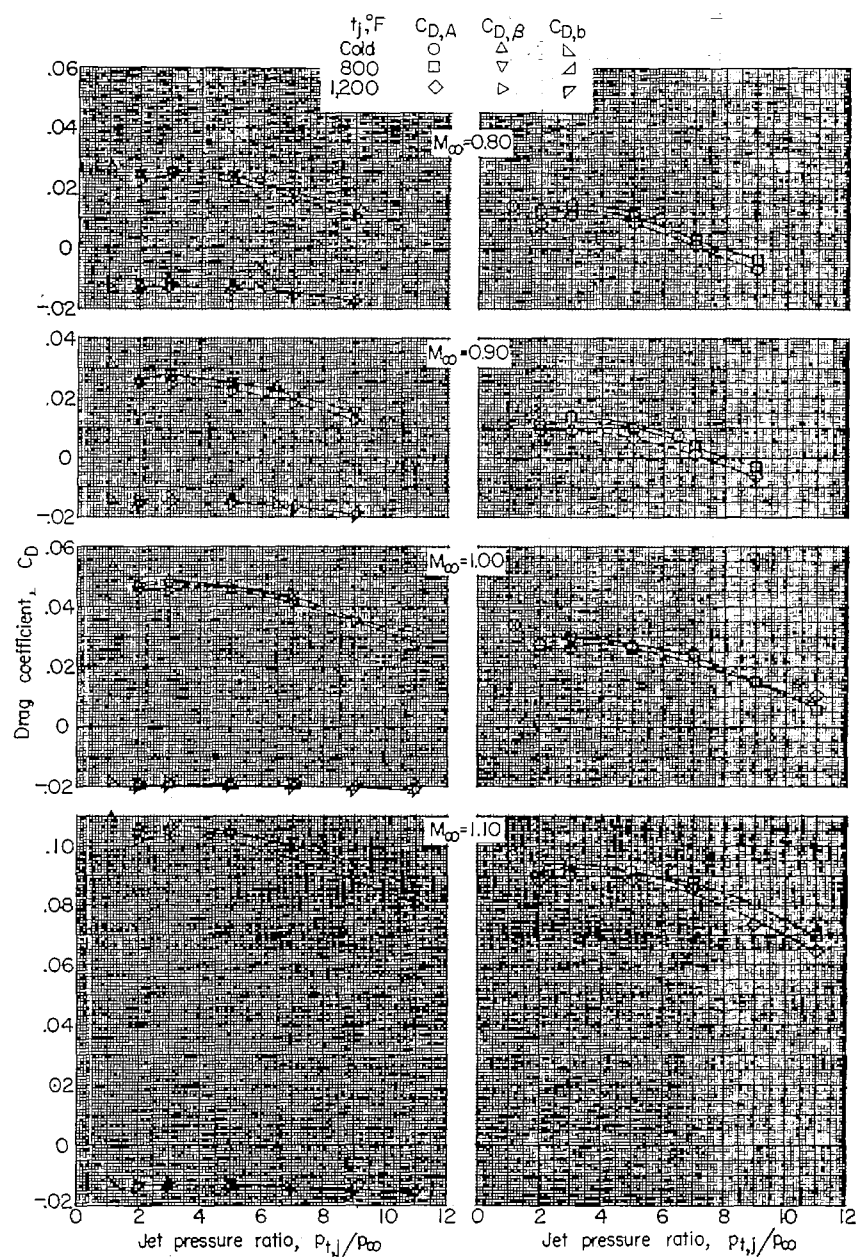
~~CONFIDENTIAL~~



(a) Afterbody I.  $\beta = 16^\circ$ ,  $\frac{d_j}{d_{\max}} = 0.248$ ,  $\frac{d_j}{d_b} = 0.742$ .

Figure 5.- Variation of base, boattail, and total afterbody pressure-drag coefficient with jet pressure ratio for different values of jet temperature and stream Mach number.



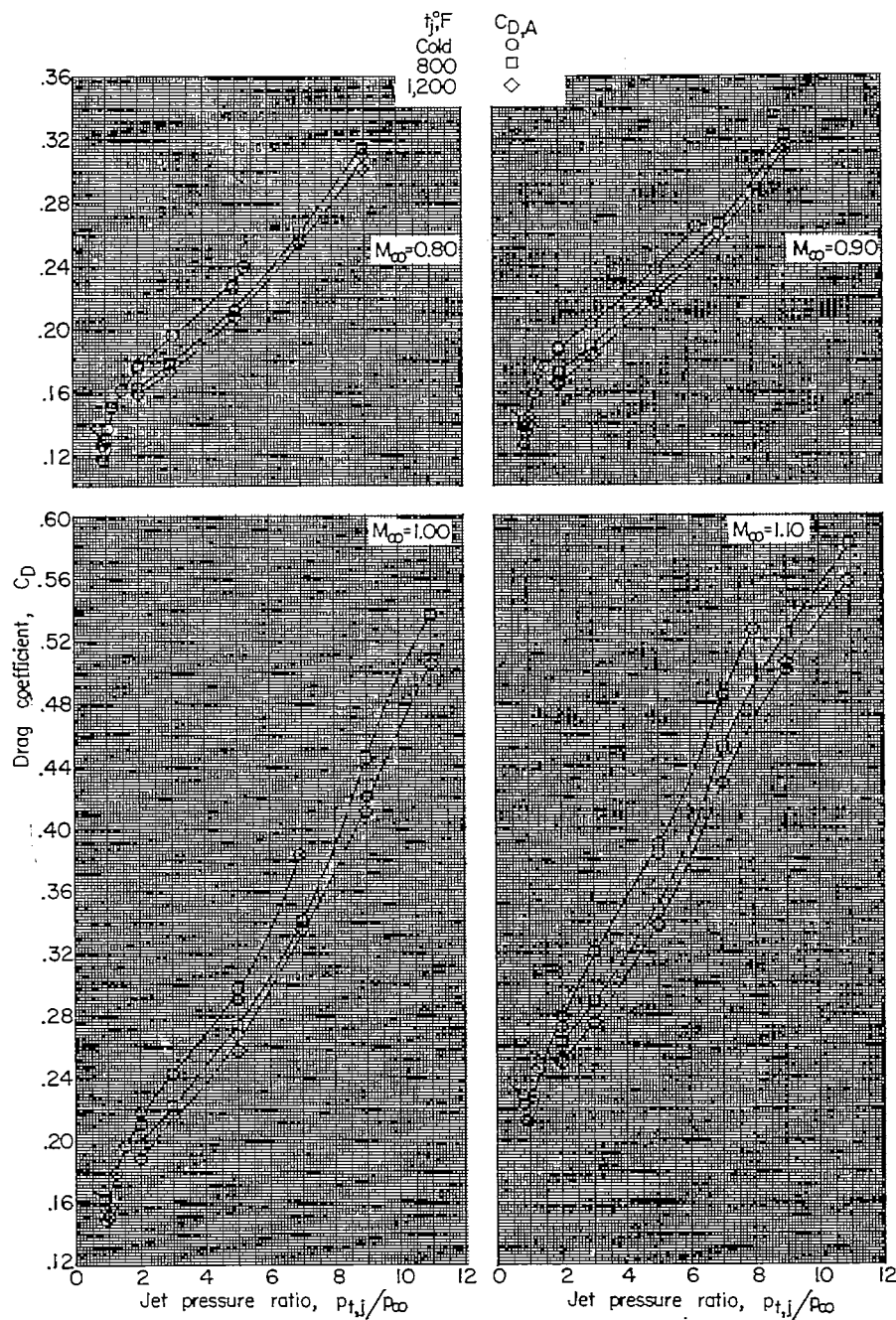


(b) Afterbody VII.  $\beta = 16^\circ$ ,  $\frac{d_j}{d_{max}} = 0.248$ ,  $\frac{d_j}{d_b} = 0.643$ .

Figure 5.- Continued.

CONFIDENTIAL

CONFIDENTIAL

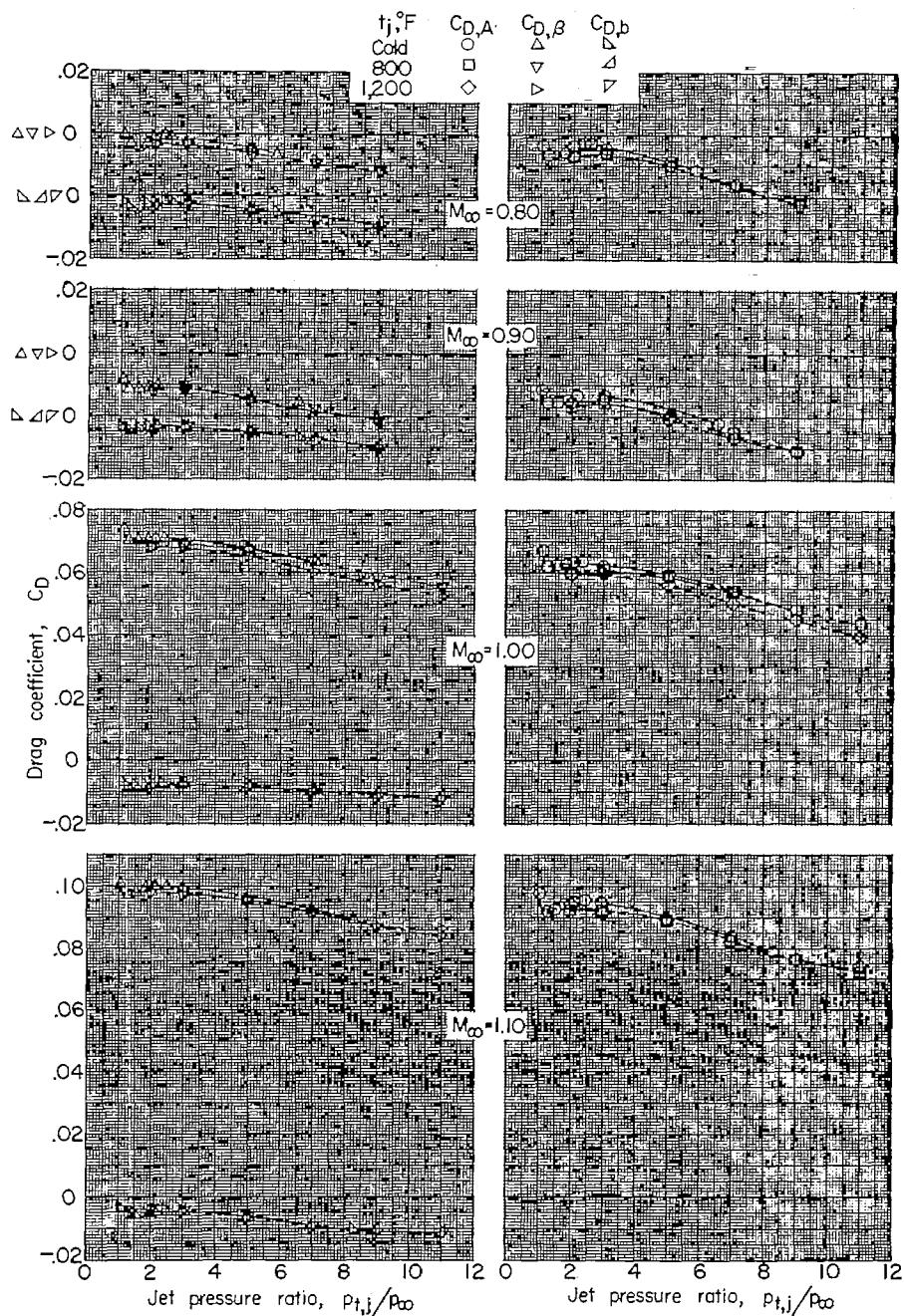


(c) Afterbody X.  $\beta = 0^\circ$ ,  $\frac{d_j}{d_{\max}} = 0.248$ ,  $\frac{d_j}{d_b} = 0.248$ . Flagged symbols are for no jet flow.

Figure 5.- Continued.

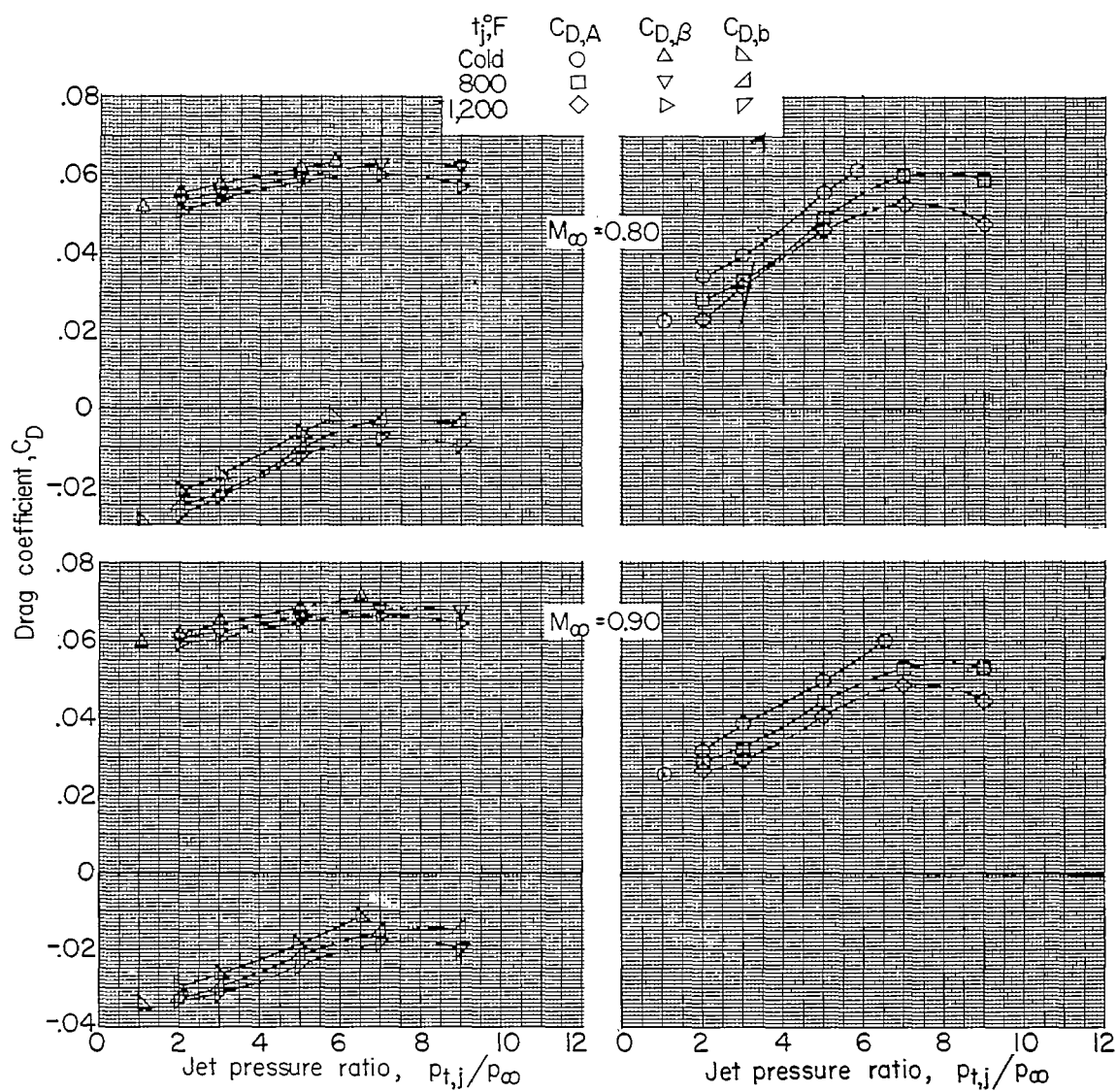
CONFIDENTIAL





(d) Afterbody XI.  $\beta = 8^\circ$ ,  $\frac{d_j}{d_{\max}} = 0.248$ ,  $\frac{d_j}{d_b} = 0.742$ .

Figure 5.- Continued.

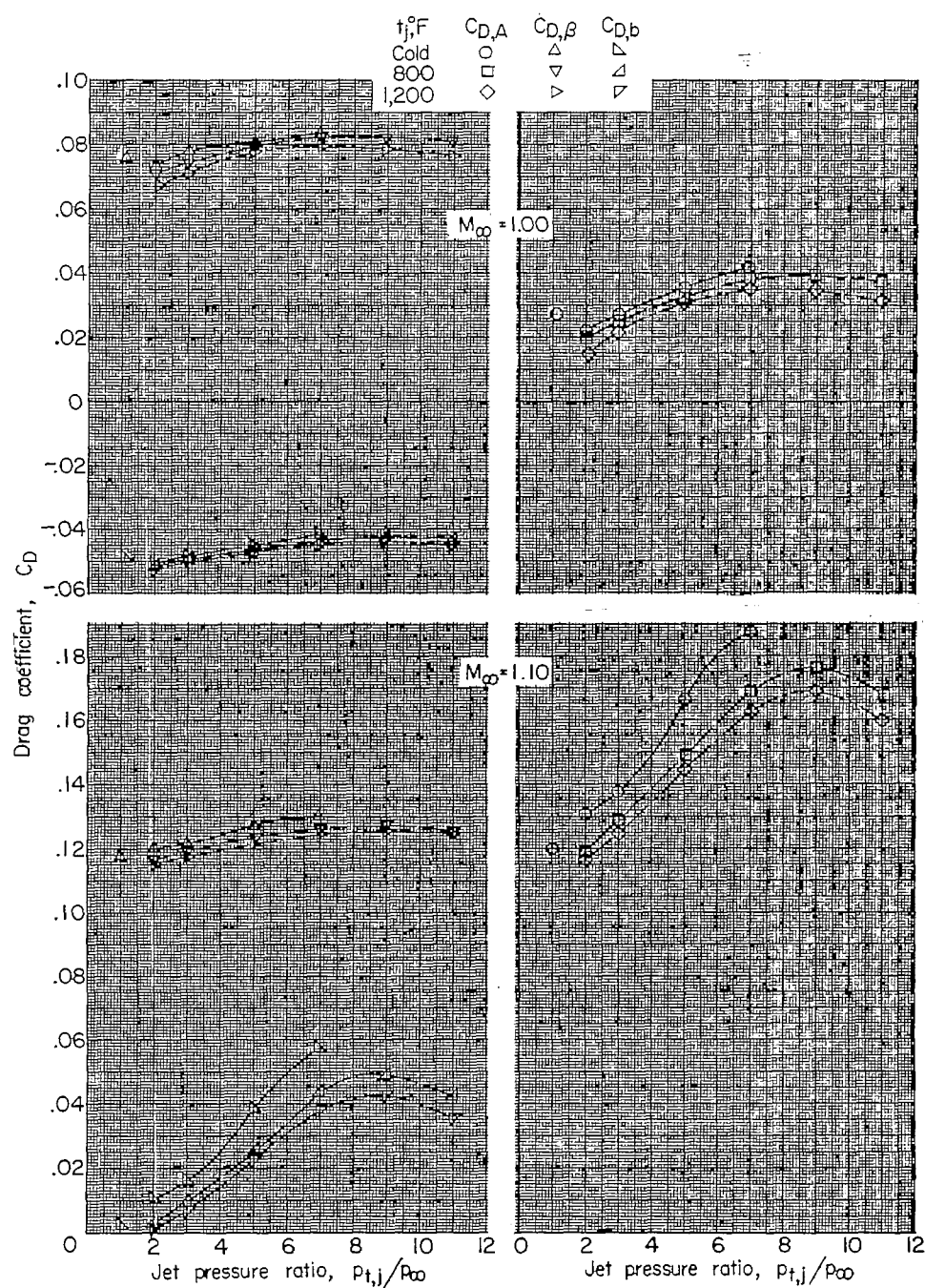


(e) Afterbody XII.  $\beta = 16^\circ$ ,  $\frac{d_j}{d_{max}} = 0.248$ ,  $\frac{d_j}{d_b} = 0.388$ .

Figure 5.- Continued.

CONFIDENTIAL

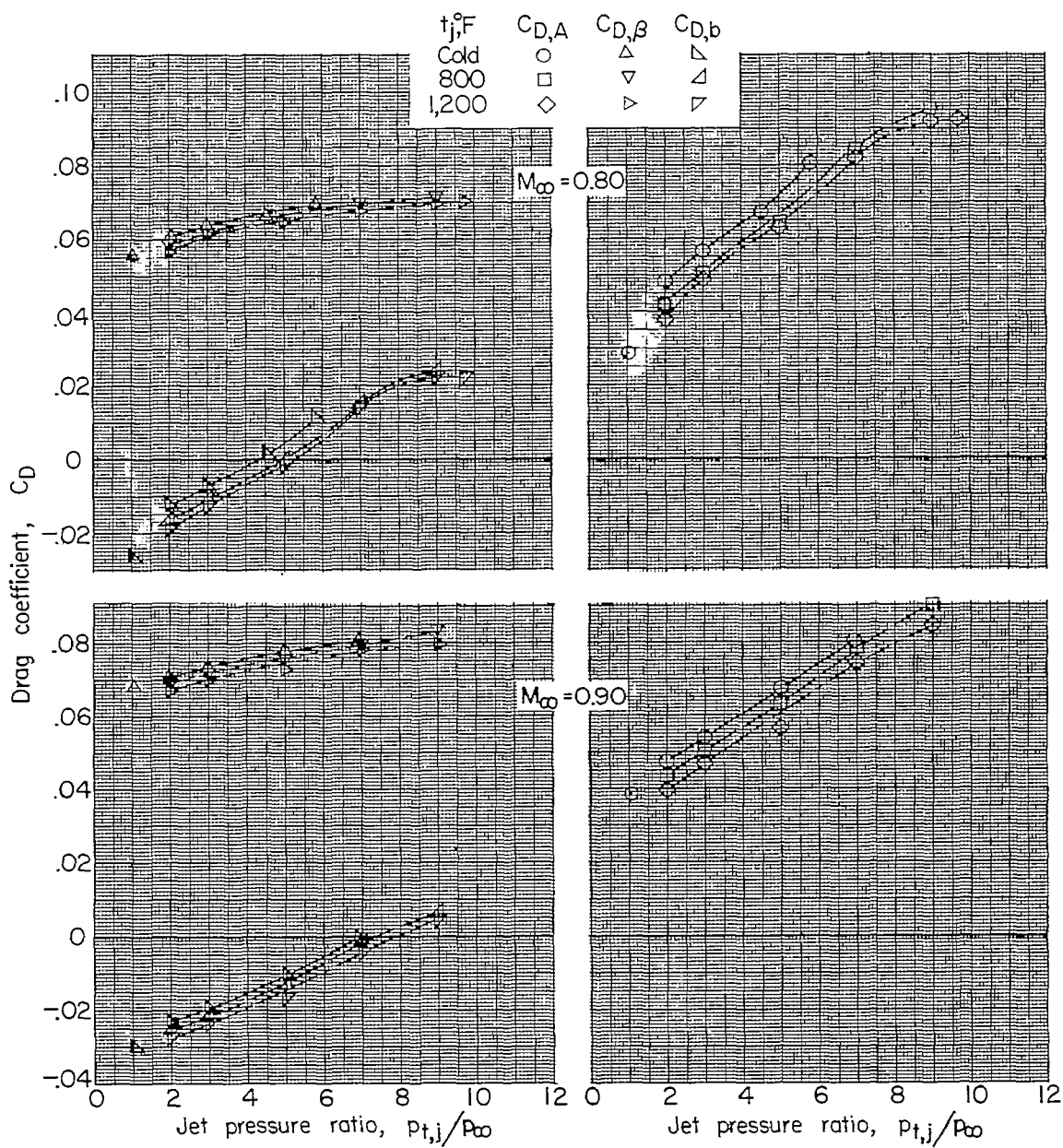
CONFIDENTIAL



(e) Concluded.

Figure 5.- Continued.

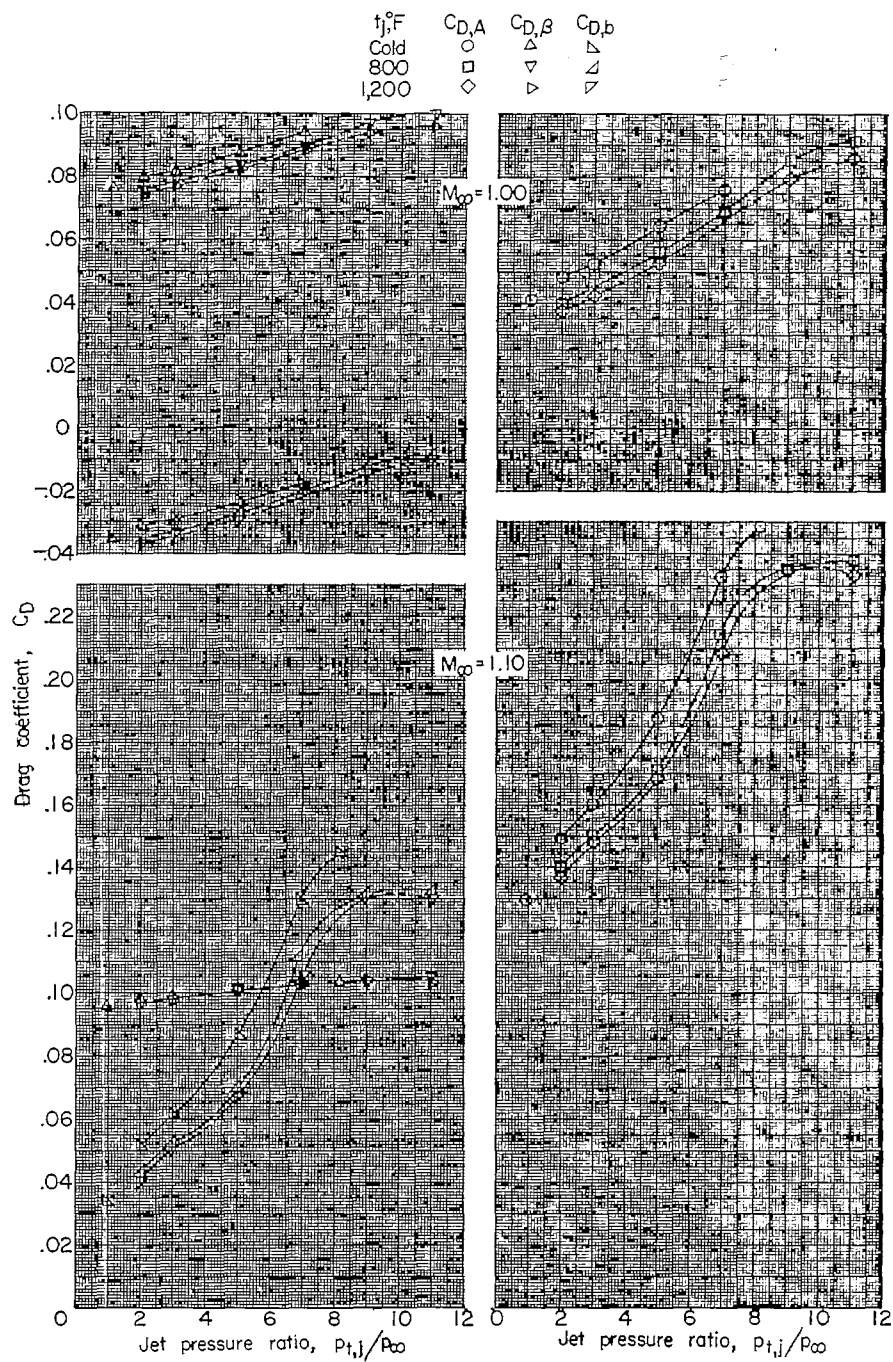
CONFIDENTIAL



(f) Afterbody XIII.  $\beta = 16^\circ$ ,  $\frac{d_j}{d_{\max}} = 0.248$ ,  $\frac{d_j}{d_b} = 0.336$ .

Figure 5.- Continued.

CONFIDENTIAL

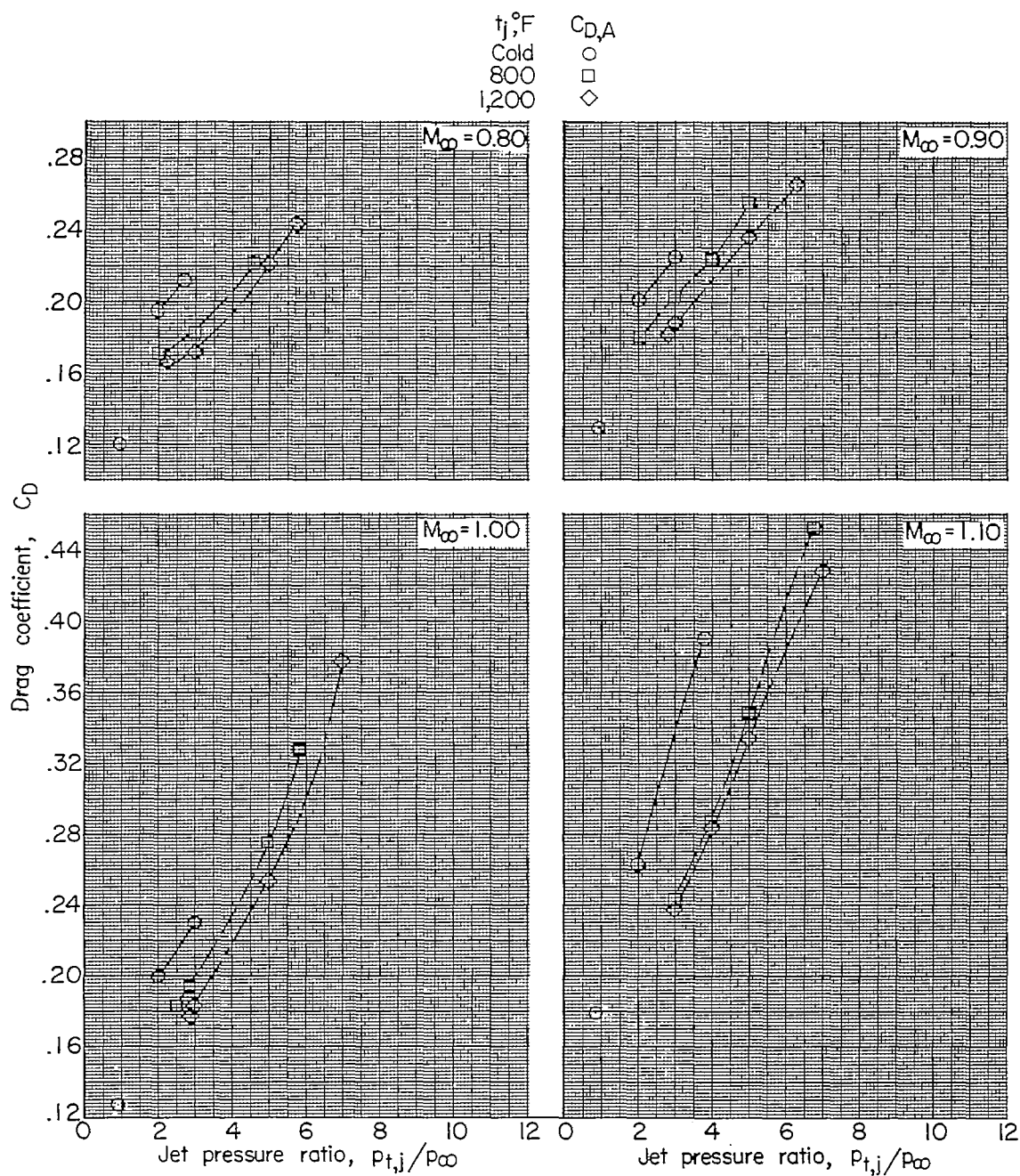
~~CONFIDENTIAL~~

(f) Concluded.

Figure 5.- Continued.

~~CONFIDENTIAL~~

CONFIDENTIAL



(g) Afterbody XIV.  $\beta = 0^\circ$ ,  $\frac{d_j}{d_{\max}} = 0.351$ ,  $\frac{d_j}{d_b} = 0.351$ .

Figure 5.- Concluded.

CONFIDENTIAL